JOURNAL OF GUIDANCE, CONTROL, AND DYNAMICS
Vol. 26, No. 3, May–June 2003

Optimal Trajectory Planning for Hot-Air Balloons in Linear Wind Fields

Tuhin Das* and Ranjan Mukherjee†
Michigan State University, East Lansing, Michigan 48824-1226
and
Jonathan Cameron‡
Jet Propulsion Laboratory, California Institute of Technology, Pasadena, California 91109

The altitude of hot-air balloons is controlled by heating the air trapped inside the balloon and allowing the air to cool naturally. Apart from controlling the altitude, it is desirable to utilize the wind field to position the balloon at a target location while minimizing fuel consumption. This can be posed as an optimal control problem with free end states, where the heat input to the system is the control variable. The problem is intractable because of the switching nature of the heat input and highly nonlinear state equations derived from the thermodynamic model of the balloon. In this paper we address the optimal control problem within a space of a few kilometers where we assume the wind fields to be known and linear. We simplify the dynamic model of the balloon and obtain optimal trajectories to the target location by solving a two-point boundary-value problem. By refining the simplified dynamic model, the accuracy of the optimal trajectories are improved to match well with trajectories obtained using the nonlinear model. Our approach based on simplification of the balloon dynamic model enables us to solve the intractable nonlinear optimal control problem and provides insight into the optimal trajectories, such as number of switchings of input and loss of accuracy for specific wind profiles. Except for these specific wind profiles, our approach yields accurate trajectories for the balloon and provides a solution to an important problem that has not been adequately addressed in the literature.

Nomenclature

A	=	cross-sectional area of sphere with volume equivalent to the balloon, m^2
C_D	=	coefficient of drag
CH_{fa}	=	convective heat-transfer coefficient between balloon film and ambient air, W/m^{2}K
CH_{gf}	=	convective heat-transfer coefficient between balloon film and balloon gas (air), W/m^{2}K
C_m	=	virtual mass coefficient
c_f	=	specific heat of the balloon film, J/kg K
c_{pg}	=	specific heat of the balloon gas (air), 1004.5 J/kg K
G	=	solar constant, 1395.0 W/m^2
Gr_a	=	Grashof number for convection between balloon film and ambient air
Gr_g	=	Grashof number for convection between balloon gas (air) and balloon film
g	=	acceleration caused by gravity, 9.81 m/s^2
K_a	=	thermal conductivity of ambient air
K_g	=	thermal conductivity of balloon gas (air)
M_a	=	molecular weight of air, 28.96 kg/kmol
m_f	=	mass of balloon film, kg
m_{fl}	=	mass of fuel, kg
m_g	=	mass of balloon gas, kg
m_{tot}	=	total mass of balloon system, kg
Nu_a	=	Nusselt number for convection between balloon film and ambient air
Nu_g	=	Nusselt number for convection between balloon gas (air) and balloon film
Pr	=	Prandtl number of air, 0.72
p_a	=	ambient air pressure, Pa
$\dot{q}_f$	=	net heat flux to balloon film, W
$\dot{q}_g$	=	net heat flux to balloon gas, W
R	=	universal gas constant, 8314.3 J/kmol K
$\bar{R}$	=	radius of a sphere with volume equivalent to the balloon, m
Re	=	Reynolds number
r_e	=	Earth relectivity (albedo), 0.18 (assuming no cloud cover)
r_w	=	reflectivity of the balloon film in the infrared spectrum
$r_{\text{w sol}}$	=	reflectivity of the balloon film to solar radiation
S	=	balloon surface area, equivalent to $4.835976\,V^{2/3}$, m^2
T_a	=	ambient air temperature, K
T_{BB}	=	blackball temperature, 214.4 K (assuming no cloud cover)
T_f	=	balloon film temperature, K
T_g	=	balloon gas temperature, K
t	=	time, s
$\mathcal{U}$	=	wind velocity in x direction, m/s
u	=	rate of heat input, W
V	=	balloon volume, m^3
$\mathcal{V}$	=	wind velocity in y direction, m/s
x	=	x coordinate of balloon, m
y	=	y coordinate of balloon, m
z	=	balloon altitude, m
α_g	=	absorptivity of balloon gas (air) to solar radiation, 0.003
α_{geff}	=	effective solar absorptivity of radiation
α_w	=	absorptivity of balloon film in the infrared spectrum
α_{weff}	=	effective solar absorptivity of the balloon film
ϵ_g	=	emmisivity of balloon gas in the infrared spectrum
ϵ_{geff}	=	effective infrared emmisivity of balloon gas
ϵ_{int}	=	effective interchange infrared emmisivity
ϵ_w	=	emmisivity of balloon film in the infrared spectrum
ϵ_{weff}	=	effective infrared emmisivity of balloon film
μ_a	=	viscosity of the ambient air, Pa s
μ_g	=	viscosity of the balloon gas (air), Pa s
ρ_a	=	density of air, kg/m^3

Received 12 July 2003; revision received 22 January 2003; accepted for publication 30 January 2003.

*Graduate Student, Department of Mechanical Engineering.
†Associate Professor, Department of Mechanical Engineering, 2555 Engineering Building.
‡Senior Engineer, 4800 Oak Grove Drive. Senior Member AIAA.

ρ_g = density of balloon gas (air), kg/m^3
σ = Stefan–Boltzmann constant, 5.669×10^{-8} W/m^{2}K^4
τ_w = transmissivity of balloon film in the infrared spectrum
$\tau_{\text{w sol}}$ = transmissivity of the balloon film to solar spectrum

I. Introduction

HOT-AIR balloons are simple and relatively inexpensive aerial vehicles that have historically been used for scientific experiments, such as precursor to manned space flight, and astronomical and telecommunications research. Its current applications include aerial surveying, probing of the upper atmosphere to provide valuable data to aircrafts, military applications, and recreation. In many of these applications, trajectory control of the balloons is important and requires proper mathematical modeling of the mechanical and thermal dynamics of the balloon. Although human operators successfully control balloons without using mathematical models, modeling will enable autonomous and semiautonomous operation with higher fuel efficiency and motion accuracy and enable trajectories that might not be conceived by human operators.

The mathematical modeling of balloons beyond simple buoyancy calculations has been largely driven by high-altitude balloon flights. Some of the early work on modeling was done by Kreider,[1] Kreith and Kreider,[2] and Carlson and Horn.[3] Their models took into account thermodynamic influences of solar and infrared radiation, as well as optical/infrared absorptivity and related radiative properties of balloon films. This is important for long flight durations and day–night transitions. The importance of vertical drafts near the surface for predicting ascent and descent motion of balloons was established by Wu and Jones.[4] The concept of buoyancy control using a phase change fluid was analyzed and demonstrated by Wu and Jones[4] and Scheid et al.[5] The primary lift in this system is provided by a classic lighter-than-air balloon. The overall lift force is modulated by a second balloon filled with a phase change fluid that remains gaseous near the ground and cools off and eventually condenses as the balloon goes up in the atmosphere.

Although thermodynamic models of balloons have been studied earlier to address the altitude control problem and recently trajectory control of balloons with lift-generating devices have been investigated (Aaron et al.[6]), flight control of balloons in the presence of lateral wind fields has not been reported. In this paper we address the trajectory control problem for hot-air balloons such that they can reach a target location by controlling their altitude and riding the wind field judiciously. A balloon typically gains height when the trapped air is heated by burning fuel. The buoyant force decreases, and the balloon starts descending when the trapped air cools naturally through heat exchange with the atmosphere. The control input of a hot-air balloon is therefore unidirectional and switches between on and off states. We design the input to minimize a weighted sum of the total fuel consumed and the error in the final coordinates of the balloon. This is motivated by the fact that very precise positioning of the balloon is not required for most applications. We assume the wind field to be known and linear and do not specify the time to be taken by the balloon to reach its destination. The knowledge of the wind field is justified by the presence of existing weather data and its linearity warranted from extrapolation of data over short distances (few kilometers). Also, in the current environment where formation flying (Folta et al.[7]) is merited as a useful concept, knowledge of wind data can be justified by measurements and sharing of data by a formation of balloons. Typically, wind data are statistical in nature, but in this paper we assume the data to be deterministic to keep the problem simple.

This paper is organized as follows. In Section II we first introduce the thermal and dynamic models of hot-air balloons from the literature. Based on certain assumptions and observations, we then derive a linear model of the balloon for the purpose of control design. The linear model enables us to cast the optimal control problem as a tractable two-point boundary-value problem and provides valuable insight into the optimal input-switching sequence, which is discussed in Section III. In Section IV we first attempt to solve the two-point boundary-value problem using a simple numerical approach. Although this approach does not have good convergence properties, it provides useful information on the scale and magnitude of the costate variables, which is a key to solving the optimal trajectories numerically. We obtain optimal trajectories using the method of relaxation (Press et al.[8]) and feed the input switching sequence into the nonlinear model of the balloon for the purpose of comparison. The linear model is refined using results from the nonlinear model and the process repeated until the nonlinear model and the relaxation algorithm yield matching trajectories. In most simulations we performed, a single iteration was sufficient to refine the linear model and obtain accurate optimal trajectories. We present simulation results in Section V and provide concluding remarks and future research directions in Section VI.

II. Mathematical Model

A. Thermal and Dynamic Model

Based on thermal and dynamic models of balloons by Carlson and Horn[3] and the coordinate system description in Fig. 1, the equations of motion of hot-air balloons can be described by the vertical force-balance equation

$$(m_{\text{tot}} + C_m \rho_a V)\frac{\mathrm{d}^2 z}{\mathrm{d}t^2} = g(\rho_a V - m_{\text{tot}}) - \frac{1}{2}\rho_a A C_D \frac{\mathrm{d}z}{\mathrm{d}t}\left|\frac{\mathrm{d}z}{\mathrm{d}t}\right| \quad (1)$$

the heat-balance equation for the balloon film

$$m_f c_f \frac{\mathrm{d}T_f}{\mathrm{d}t} = \dot{q}_f \quad (2)$$

and the heat-balance equation for the lifting gas (hot air)

$$m_g c_{\text{pg}} \frac{\mathrm{d}T_g}{\mathrm{d}t} = \dot{q}_g - \left(\frac{g m_g T_g}{T_a}\right)\frac{\mathrm{d}z}{\mathrm{d}t} + u \quad (3)$$

where

$$V = \frac{m_g R T_g}{p_a M_a}, \qquad m_{\text{tot}} \triangleq m_g + m_f + m_{\text{fl}}, \qquad A = \pi \bar{R}^2 \quad (4)$$

The heat-flux terms $\dot{q}_f$ and $\dot{q}_g$ in Eqs. (2) and (3) can be expressed as

$$\dot{q}_f = \left[G\alpha_{\text{weff}}(1/4 + r_e/2) + \epsilon_{\text{int}}\sigma\left(T_g^4 - T_f^4\right) + CH_{\text{gf}}(T_g - T_f) + CH_{\text{fa}}(T_a - T_f) - \epsilon_{\text{weff}}\sigma T_f^4 + \epsilon_{\text{weff}}\sigma T_{\text{BB}}^4\right]S \quad (5)$$

$$\dot{q}_g = \left[G\alpha_{\text{geff}}(1 + r_e) - \epsilon_{\text{int}}\sigma\left(T_g^4 - T_f^4\right) - CH_{\text{gf}}(T_g - T_f) - \epsilon_{\text{geff}}\sigma T_g^4 + \epsilon_{\text{geff}}\sigma T_{\text{BB}}^4\right]S \quad (6)$$

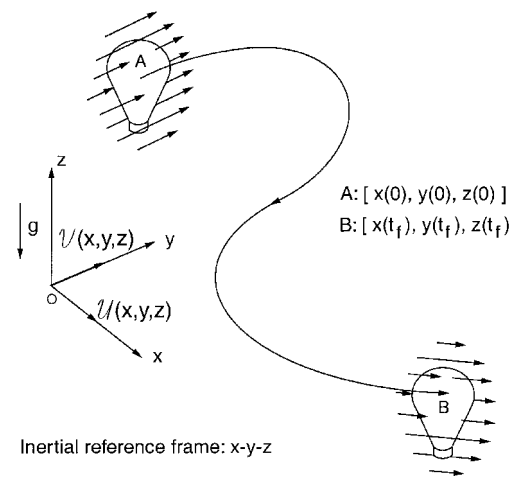

Fig. 1 Trajectory of a hot-air balloon in a wind field.

where

$$\alpha_{\text{weff}} = \alpha_w\left[1 + \frac{\tau_{\text{wsol}}(1-\alpha_g)}{1 - r_{\text{wsol}}(1-\alpha_g)}\right], \qquad \alpha_{\text{geff}} = \frac{\alpha_g \tau_{\text{wsol}}}{1 - r_{\text{wsol}}(1-\alpha_g)}$$

$$\epsilon_{\text{int}} = \frac{\epsilon_g \epsilon_w}{1 - r_w(1-\epsilon_g)}, \qquad \epsilon_{\text{geff}} = \frac{\epsilon_g \tau_w}{1 - r_w(1-\epsilon_g)}$$

$$\epsilon_{\text{weff}} = \epsilon_w\left[1 + \frac{\tau_w(1-\epsilon_g)}{1 - r_w(1-\epsilon_g)}\right] \tag{7}$$

and $S = 4\pi \bar{R}^2$. The expressions for ϵ_g, CH_{fa}, and CH_{gf} are given in the Appendix. The motion of the balloon in the x and y directions is caused by wind drag and can be approximated by the equations

$$\dot{x} = \gamma \mathcal{U}, \qquad \dot{y} = \gamma \mathcal{V} \tag{8}$$

where γ is the ratio of the balloon speed and the absolute wind speed and is a measure of drag. Because our wind field is linear, $\mathcal{U}$ and $\mathcal{V}$ can be described by the equations

$$\mathcal{U} = \mathcal{U}_0 + k_{11}(x - x_0) + k_{12}(y - y_0) + k_{13}(z - z_0) \tag{9a}$$

$$\mathcal{V} = \mathcal{V}_0 + k_{21}(x - x_0) + k_{22}(y - y_0) + k_{23}(z - z_0) \tag{9b}$$

where $\mathcal{U}_0$ and $\mathcal{V}_0$ are the x and y components of the wind velocity at the initial location of the balloon (x_0, y_0, z_0), and the parameters k_{ij}, $i = 1, 2$, $j = 1, 2, 3$ are constants. The velocity of the wind in the vertical direction is assumed to be zero.

B. Model Simplification for Control Problem Formulation

The intricately coupled thermal and dynamic equations of the balloon in Eqs. (1–3), (5), (6), and (8) can be represented in the standard state-space form

$$\dot{\boldsymbol{X}} = \boldsymbol{f}(\boldsymbol{X}, u) \tag{10}$$

where $\boldsymbol{X}$ is the vector of state variables and $\boldsymbol{f}$ is a nonlinear vector function of the states and the input. Our goal is to obtain the optimal input u that minimizes the cost funtional

$$J = \phi[\boldsymbol{X}(t_f)] + \int_0^{t_f} L(\boldsymbol{X}, u)\, \mathrm{d}t \tag{11}$$

where ϕ is a measure of the error in the Cartesian coordinates of the balloon at the final time $t = t_f$. The term $\phi[\boldsymbol{X}(t_f)]$ is included in the cost function because a fixed end-state problem will be ill posed with the balloon having no direct control in the x and y directions. The Lagrangian function L was chosen as the fuel consumed by the balloon such that the cost function is a weighted sum of the total fuel consumed and the terminal error. The equations for the costates or adjoint variables can be written as (Lewis and Syrmos[9])

$$\dot{\boldsymbol{\lambda}}^T = -\frac{\partial H}{\partial \boldsymbol{X}}, \qquad \boldsymbol{\lambda}^T(t_f) = \left(\frac{\partial \phi}{\partial \boldsymbol{X}}\right)_{t_f}, \qquad H \triangleq L + \boldsymbol{\lambda}^T \boldsymbol{f} \tag{12}$$

where H is the Hamiltonian. The optimal input can be obtained by minimizing the Hamiltonian over admissible choices of the input, which essentially has on and off states. This poses an extremely difficult problem for our nonlinear system in which the costate equations are very complicated. To make the problem tractable, we make a few assumptions, some of them based on observations, that essentially result in linearization of the dynamic and thermodynamic equations. These assumptions are discussed next:

1) The term $(m_{\text{tot}} + C_m \rho_a V)$ in Eq. (1) is assumed to be constant. This assumption is reasonable because the fractional change in mass of the balloon caused by consumption of fuel and change in volume is quite insignificant. The value of the constant is determined from initial conditions.

2) The cross-sectional area of the balloon A is assumed to be constant. This allows further simplification of Eq. (1).

3) The variation in ambient temperature and pressure is assumed to be small over the range of travel of the balloon. Both T_a and p_a are therefore treated as constants. This implies that ρ_a is also constant.

4) We now focus our attention on the drag term in Eq. (1) involving $\dot{z}|\dot{z}|$. This term increases as the square of the velocity and therefore has a limiting effect on the velocity of the balloon. Assuming the balloon velocity to satisy $|\dot{z}| \le \dot{z}_{\max}$, we can approximate the drag term using the method of least squares (Kreyszig[10]) by minimizing the integral

$$I = \int_{-\dot{z}_{\max}}^{+\dot{z}_{\max}} (\dot{z}|\dot{z}| - k\dot{z})^2\, \mathrm{d}\dot{z}$$

with respect to k. This results in the approximation

$$\dot{z}|\dot{z}| \approx k\dot{z}, \qquad k \triangleq 0.75\dot{z}_{\max} \tag{13}$$

The equation used for modeling drag in x and y directions, namely, Eq. (8), is different from Eq. (1), which models drag in the z direction. We chose the simpler drag model in x and y directions simply because it reduces the dimension of the problem by two states and two costates. The choice of a simpler model is also justified by the fact that the balloon dynamics in the x and y directions are much less complicated than the dynamics of the balloon in the z direction.

5) The most significant and key assumption in this paper pertains to linearization of the heat-balance equations, namely, Eqs. (2) and (3). It is evident from Eqs. (5) and (6) that the terms $\dot{q}_f$ and $(\dot{q}_g - g m_g T_g \dot{z}/T_a)$ in Eqs. (2) and (3) are nonlinear functions of $\dot{z}$, T_f, and T_g. To express them in linear form, we express them as

$$-\dot{q}_f = a_1\dot{z} + b_1 T_f + c_1 T_g \tag{14a}$$

$$-\dot{q}_g + g m_g T_g \dot{z}/T_a = a_2\dot{z} + b_2 T_f + c_2 T_g \tag{14b}$$

and identify the constants a_1, b_1, c_1, a_2, b_2, and c_2 from simulation results using the method of least squares (Kreyszig[10]). The simulation results indicate an excellent match between the left- and right-hand sides of both Eqs. (14a) and (14b) and affirm the accuracy of the linear representation.

To demonstrate the advantages of linearization of the heat-flux equations, we present results from two simulation maneuvers. The parameters used in simulation are provided in Section V. In the first simulation the balloon was commanded to hover at 12 km starting from an initial altitude of 14 km. The hover was achieved by simply switching on the heat input when the balloon was below the hover altitude and had a downward vertical velocity. Figure 2a shows that the balloon initially drops below the hover altitude, then rises back up slowly, and finally hovers at 12 km. The least-squares coefficients were obtained as

$$a_1 = 0.236625 \times 10^4, \qquad a_2 = 8.152573 \times 10^3$$

$$b_1 = 0.282035 \times 10^4, \qquad b_2 = -2.344357 \times 10^3$$

$$c_1 = -0.257485 \times 10^4, \qquad c_2 = 2.272179 \times 10^3$$

These coefficients were substituted in Eq. (14) to obtain linear approximation of the terms $-\dot{q}_f$ and $(-\dot{q}_g + g m_g T_g \dot{z}/T_a)$; the results are shown in Figs. 2b and 2c in dashed lines. These plots are almost indistinguishable from the plots of $-\dot{q}_f$ and $(-\dot{q}_g + g m_g T_g \dot{z}/T_a)$ obtained from the simulation of the nonlinear model, shown in solid lines.

We present results of one more simulation to be convinced of the accuracy of linear approximation of the thermodynamic equations. In this simulation the heat input was switched on and off multiple times in an arbitrary manner. The balloon altitude is shown in Fig. 3a, and the plots of $-\dot{q}_f$ and $(-\dot{q}_g + g m_g T_g \dot{z}/T_a)$ are shown in Figs. 3b and 3c. These plots once again indicate that the linear heat-flux terms approximate their actual variation very closely. The least-squares

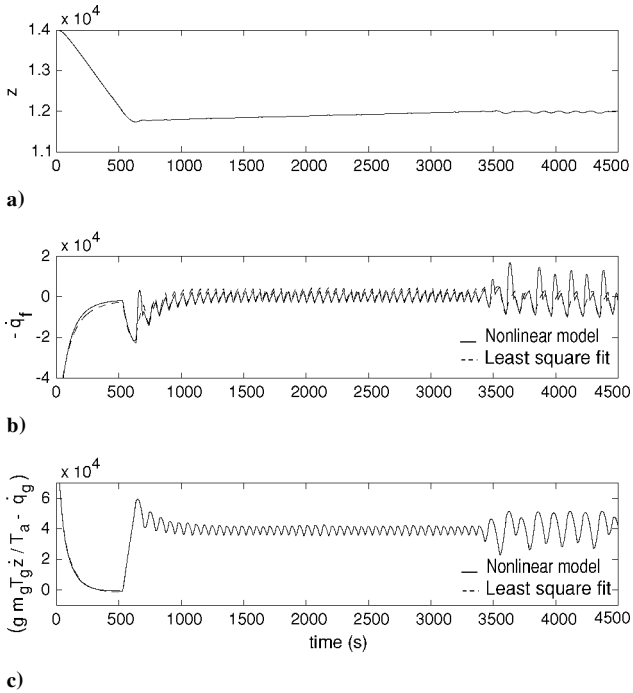

Fig. 2 Least-squares fit for heat-flux terms for a hover maneuver.

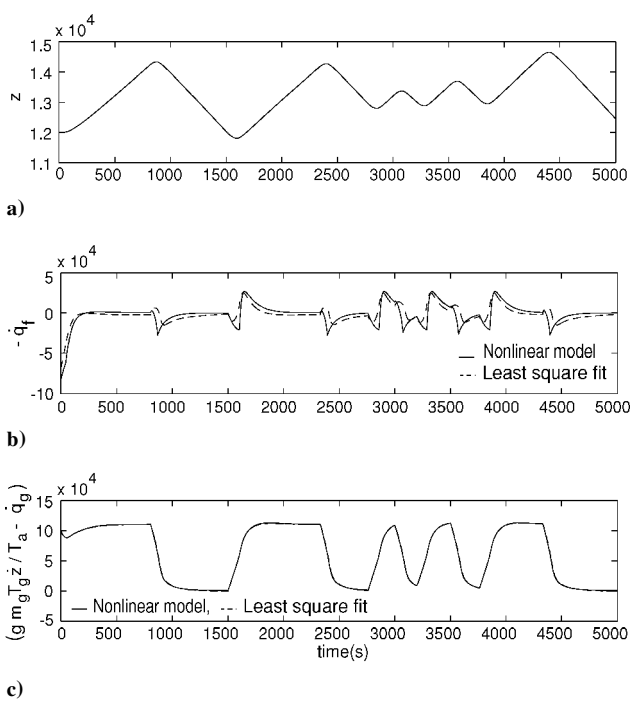

Fig. 3 Least-squares fit for heat-flux terms for another maneuver.

coefficients were obtained as

$$a_1 = 1.187972 \times 10^4, \qquad a_2 = 8.179336 \times 10^3$$

$$b_1 = 0.432366 \times 10^4, \qquad b_2 = -2.501151 \times 10^3$$

$$c_1 = -0.383053 \times 10^4, \qquad c_2 = 2.414179 \times 10^3$$

III. Optimal Control Formulation

A. Linear State-Space Representation

Based on the assumptions made in the preceding section, we can now express the dynamical and thermodynamical equations of the balloon in the linear state-space form

$$\dot{\boldsymbol{X}} = \boldsymbol{A}\boldsymbol{X} + \boldsymbol{B}u, \qquad \boldsymbol{X}(0) = \boldsymbol{X}_0 \tag{15}$$

where the state vector $\boldsymbol{X}$ and matrix $\boldsymbol{A}$ are defined as

$$\boldsymbol{X} \triangleq \begin{bmatrix} \bar{x} \\ \bar{y} \\ \bar{z} \\ \dot{\bar{z}} \\ T_f \\ V \\ x_7 \\ x_8 \\ x_9 \end{bmatrix}$$

$$\boldsymbol{A} \triangleq \begin{bmatrix} \gamma k_{11} & \gamma k_{12} & \gamma k_{13} & 0 & 0 & 0 & 0 & 1 & 0 \\ \gamma k_{21} & \gamma k_{22} & \gamma k_{23} & 0 & 0 & 0 & 0 & 0 & 1 \\ 0 & 0 & 0 & 1 & 0 & 0 & 0 & 0 & 0 \\ 0 & 0 & 0 & p_1 & 0 & p_2 & -1 & 0 & 0 \\ 0 & 0 & 0 & -\bar{a}_1 & -\bar{b}_1 & -\bar{c}_1 & 0 & 0 & 0 \\ 0 & 0 & 0 & -\bar{a}_2 & -\bar{b}_2 & -\bar{c}_2 & 0 & 0 & 0 \\ 0 & 0 & 0 & 0 & 0 & 0 & 0 & 0 & 0 \\ 0 & 0 & 0 & 0 & 0 & 0 & 0 & 0 & 0 \\ 0 & 0 & 0 & 0 & 0 & 0 & 0 & 0 & 0 \end{bmatrix},$$

$$\boldsymbol{B} \triangleq \begin{bmatrix} 0 \\ 0 \\ 0 \\ 0 \\ 0 \\ R/p_a M_g c_{\mathrm{pg}} \\ 0 \\ 0 \\ 0 \end{bmatrix} \tag{16}$$

and $\boldsymbol{X}_0$ is the state vector at the initial time $t = 0$. In Eq. (16) the first three states are defined as $\bar{x} \triangleq (x - x_d)$, $\bar{y} \triangleq (y - y_d)$, $\bar{z} \triangleq (z - z_d)$, where x_d, y_d, z_d are the desired Cartesian coordinates of the balloon, and the last three states are constants, given by the relations

$$x_7 \triangleq m_{\mathrm{tot}} g/(m_{\mathrm{tot}} + C_m \rho_a V), \qquad x_8 \triangleq \gamma(\mathcal{U}_0 - k_{11}x_0 - k_{12}y_0)$$

$$x_9 \triangleq \gamma(\mathcal{V}_0 - k_{21}x_0 - k_{22}y_0) \tag{17}$$

In Eq. (16) we also have $p_1 \triangleq -0.5k\rho_a C_D A/(m_{\mathrm{tot}} + C_m \rho_a V)$, $p_2 \triangleq g\rho_a/(m_{\mathrm{tot}} + C_m \rho_a V)$, and

$$\bar{a}_1 \triangleq a_1/m_f c_f, \qquad \bar{a}_2 \triangleq a_2 R/p_a m_g c_{\mathrm{pg}}$$

$$\bar{b}_1 \triangleq b_1/m_f c_f, \qquad \bar{b}_2 \triangleq b_2 R/p_a m_g c_{\mathrm{pg}}$$

$$\bar{c}_1 \triangleq c_1\, p_a M_a/m_f c_f m_g R, \qquad \bar{c}_2 \triangleq c_2/m_g c_{\mathrm{pg}} \tag{18}$$

where the constants $a_1, a_2, b_1, b_2, c_1, c_2$ were defined in Eq. (14). In our model, the volume of the balloon V is one of the state variables. Because V and T_g are related by the algebraic expression in Eq. (4), T_g can be alternatively used as the state variable instead of V.

To proceed with our analysis, we express the cost function in Eq. (11) as follows:

$$J = \frac{1}{2}\boldsymbol{X}^T(t_f)\boldsymbol{F}\boldsymbol{X}(t_f) + \frac{\beta}{2}\int_0^{t_f} u^2\,\mathrm{d}t \tag{19}$$

where $\boldsymbol{F} \triangleq \mathrm{diag}(1 \quad 1 \quad 1 \quad 0 \quad 0 \quad 0 \quad 0 \quad 0 \quad 0)$ is a diagonal positive semidefinite matrix chosen to penalize the terminal error in the Cartesian coordinates of the balloon, all of them equally, and β is

a positive scalar representing the fuel cost. The Hamiltonian and costate equations can now be obtained from Eqs. (12) and (15) as follows:

$$H = (\beta/2)u^2 + \boldsymbol{\lambda}^T(\boldsymbol{AX} + \boldsymbol{B}u)$$

$$= (\beta/2)u^2 + (\lambda_6 R/p_a M_g c_{\text{pg}})u + \boldsymbol{\lambda}^T\boldsymbol{AX} \tag{20}$$

$$\dot{\boldsymbol{\lambda}} = -\boldsymbol{A}^T\boldsymbol{\lambda}, \qquad \boldsymbol{\lambda}(t_f) = \boldsymbol{FX}(t_f) \tag{21}$$

The optimal input is obtained by minimizing the Hamiltonian in Eq. (20) for admissible choices of the input. If we assume u to switch between values 0 and η, where η is the heat added to the balloon gas when the input is on, the optimal input can be expressed as follows:

$$u = \begin{cases} 0, & \text{if} \quad \lambda_6 R/(c_{\text{pg}}\, p_a M_g \beta) > -0.5\eta \\ \eta, & \text{if} \quad \lambda_6 R/(c_{\text{pg}}\, p_a M_g \beta) \le -0.5\eta \end{cases} \tag{22}$$

This indicates that the optimal input depends only on the trajectory of the costate λ_6, and switching occurs when

$$\lambda_6 = -0.5\eta c_{\text{pg}} p_a M_g \beta / R \tag{23}$$

B. Insight into Optimal Trajectories

In the absence of linearization the states and costates are described by coupled nonlinear differential equations, and it is not possible to obtain an analytical expression for the optimal input. By linearization of the balloon dynamics, we are able to get an analytical expression for the optimal input, namely, Eq. (22), and represent the states and costates in a cascade form, where the costates depend on themselves and the states depend on both the state and costate variables. This reduces the computational complexity of the two-point boundary-value problem and provides useful insight into the optimal trajectories. To obtain this insight, we first observe that λ_6 depends only on the first six costates. Because the optimal input depends on λ_6, we only need to analyze the trajectories of the first six costates. These trajectories can be described by the differential equations and boundary conditions

$$\begin{bmatrix} \dot{\lambda}_1 \\ \dot{\lambda}_2 \\ \dot{\lambda}_3 \\ \dot{\lambda}_4 \\ \dot{\lambda}_5 \\ \dot{\lambda}_6 \end{bmatrix} = \begin{bmatrix} -\gamma k_{11} & -\gamma k_{21} & 0 & 0 & 0 & 0 \\ -\gamma k_{12} & -\gamma k_{22} & 0 & 0 & 0 & 0 \\ -\gamma k_{13} & -\gamma k_{23} & 0 & 0 & 0 & 0 \\ 0 & 0 & -1 & -p_1 & \bar{a}_1 & \bar{a}_2 \\ 0 & 0 & 0 & 0 & \bar{b}_1 & \bar{b}_2 \\ 0 & 0 & 0 & -p_2 & \bar{c}_1 & \bar{c}_2 \end{bmatrix} \begin{bmatrix} \lambda_1 \\ \lambda_2 \\ \lambda_3 \\ \lambda_4 \\ \lambda_5 \\ \lambda_6 \end{bmatrix},$$

$$\begin{bmatrix} \lambda_1 \\ \lambda_2 \\ \lambda_3 \\ \lambda_4 \\ \lambda_5 \\ \lambda_6 \end{bmatrix}_{t_f} = \begin{bmatrix} \bar{x}(t_f) \\ \bar{y}(t_f) \\ \bar{z}(t_f) \\ 0 \\ 0 \\ 0 \end{bmatrix} \tag{24}$$

The preceding costate equations can also be written as

$$\begin{bmatrix} \dot{\lambda}_1 \\ \dot{\lambda}_2 \end{bmatrix} = \boldsymbol{M}_1 \begin{bmatrix} \lambda_1 \\ \lambda_2 \end{bmatrix}, \qquad \boldsymbol{M}_1 \triangleq -\gamma \begin{bmatrix} k_{11} & k_{21} \\ k_{12} & k_{22} \end{bmatrix}$$

$$\dot{\lambda}_3 = -\gamma k_{13}\lambda_1 - \gamma k_{23}\lambda_2$$

$$\begin{bmatrix} \dot{\lambda}_4 \\ \dot{\lambda}_5 \\ \dot{\lambda}_6 \end{bmatrix} = \boldsymbol{M}_2 \begin{bmatrix} \lambda_4 \\ \lambda_5 \\ \lambda_6 \end{bmatrix} + \begin{bmatrix} -1 \\ 0 \\ 0 \end{bmatrix} \lambda_3, \qquad \boldsymbol{M}_2 \triangleq \begin{bmatrix} -p_1 & \bar{a}_1 & \bar{a}_2 \\ 0 & \bar{b}_1 & \bar{b}_2 \\ -p_2 & \bar{c}_1 & \bar{c}_2 \end{bmatrix} \tag{25}$$

which indicates that the expression for λ_6 will have the form

$$\lambda_6 = C_1 e^{\alpha_1 t} + C_2 e^{\alpha_2 t} + C_3 e^{\alpha_3 t} + C_4 e^{\alpha_4 t} + C_5 e^{\alpha_5 t} \tag{26}$$

if the eigenvalues of $\boldsymbol{M}_1$ and $\boldsymbol{M}_2$ are distinct. In Eq. (26) C_i and α_i, $i = 1, 2, 3, 4, 5$ are arbitrary constants and eigenvalues of $\boldsymbol{M}_1$ and $\boldsymbol{M}_2$, respectively. If all of the eigenvalues are additionally real, Eq. (26) implies that the switching condition in Eq. (23) can occur at most four times (Leitmann[11]). The matrix $\boldsymbol{M}_1$ will have real eigenvalues if there exist no vortices in the wind field. This might be a reasonable assumption because vortices can cause the balloon to be trapped in a fixed region. Because entries of $\boldsymbol{M}_2$ depend on physical parameters of the balloon, $\boldsymbol{M}_2$ will have real eigenvalues depending on values of these parameters. The knowledge of the maximum number of switchings provides insight into the balloon trajectories because one can now conjure up wind fields that will cause the heat input to switch one, two, three, or four times. If $\boldsymbol{M}_1$ and $\boldsymbol{M}_2$ have imaginary eigenvalues, there could be more switchings—the number of switchings will however be finite because our problem has a fixed time.

IV. Solution of Two-Point Boundary-Value Problem

A. Simple Numerical Approach

The optimal control problem of the hot-air balloon, described by Eqs. (15), (22), and (24), results in a two-point boundary-value problem. Because it imposes constraints on the control input and does not admit a closed-form analytical solution like the linear quadratic regulator problem, it has to be solved numerically. We provide a simple numerical approach for solving the boundary-value problem in this section. The approach is similar to the shooting method (Press et al.[8]) and is described by the following steps:

1) We make an initial guess of the first three states at the final time, namely, $\bar{x}(t_f)$, $\bar{y}(t_f)$, $\bar{z}(t_f)$. This gives us the boundary conditions for the costates at $t = t_f$, as shown in Eq. (24).

2) Integrate Eq. (24) backward in time to obtain the costate trajectories.

3) Determine the input switching sequence from the trajectory of λ_6 and Eq. (22).

4) Use this input profile to integrate Eq. (15) forward in time and determine the values of the first three states at the final time.

5) Compute the error between values of $\bar{x}(t_f)$, $\bar{y}(t_f)$, $\bar{z}(t_f)$ obtained in step 4 and their values assumed in step 1. Make appropriate changes in the assumed values using the method of steepest descent (Press et al.[8]) and repeat steps 1–4 until the error converges to zero.

The method just discussed is easy to implement but often reaches a local minima and therefore fails to converge. It nevertheless provides us with a clear idea of the scale and magnitude of the costate variables. This knowledge is critical in computing the optimal trajectories numerically using the relaxation method (Press et al.[8]). The relaxation method, which is discussed in the next section, has been successfully used in solving other complex nonlinear aerospace optimal control problems, for example, see Ref. 12.

B. Solution by Relaxation Method

In the relaxation method ordinary differential equations (ODEs) are replaced by finite difference equations (FDEs) on a grid or mesh of points that spans the domain of interest. When the problem involves N coupled first-order ODEs represented by FDEs on a mesh of M points, there are N variables at each of the M mesh points. With $N \times M$ variables altogether the method involves inverting an $MN \times MN$ matrix, but the matrix takes a special block diagonal form that allows an economical inversion both in terms of time and storage. The solution of the FDE problem starts with an initial guess for $x_{n,k}$, $n = 1, 2, \ldots, N$, $k = 1, 2, \ldots, M$. Then the increments $\Delta x_{n,k}$ are determined such that $x_{n,k} + \Delta x_{n,k}$ is an improved approximation. This is done by a first-order Taylor-series expansion, the details of which can be found in the book by Press et al.[8] After each iteration an average correction error is computed by summing the absolute values of all corrections, weighted by a scale factor appropriate to each variable:

$$err = \frac{1}{M \times N} \sum_{k=1}^{N} \sum_{j=1}^{N} \frac{\Delta X(j,k)}{scalv(j)}$$

where *scalv* is an array that contains the typical size of the state and costate variables. The numerical method discussed in Sec. IV.A was very useful in estimating the entries of *scalv* for the costate variables, and our success with the relaxation method can be partially attributed to it. The relaxation method converges when the value of *err* becomes less than a small preselected value, and we were able to get convergence for all simulations that we attempted.

We now provide a summary of the steps taken in implementation of the relaxation algorithm:

1) The first step is to make a good initial guess of the parameters $\bar{a}_1$, $\bar{b}_1$, $\bar{c}_1$, $\bar{a}_2$, $\bar{b}_2$, $\bar{c}_2$ in Eq. (18). Because these parameters are dependent on the heat input sequence, their correct values are initially unknown. A good first estimate of the parameter values is obtained from a hover maneuver of the balloon in the neighborhood of its initial altitude.

2) The parameter values obtained in step 1 are used in the relaxation algorithm to obtain the heat input switching sequence and the corresponding trajectory of the balloon.

3) The input switching sequence in step 2 is fed into the nonlinear model of the balloon and the resulting trajectory compared with the trajectory obtained in step 2. If the two trajectories are very similar, the input switching sequence in step 2 is optimal.

4) If the balloon trajectories obtained in steps 2 and 3 are not similar, the linear model of the balloon needs to be refined. To this end, we use results obtained from the nonlinear model in step 3 to better estimate the parameters in step 1. Steps 2, 3, and 4 are then repeated until the trajectories obtained from the linear and nonlinear models match closely.

V. Simulation Results

To demonstrate the efficacy of the iterative algorithm discussed in Sec. IV.B, we present simulation results. The dynamic parameters of the balloon are assumed to be

$$m_g = 600, \qquad m_f = 200, \qquad m_{\text{fl}} = 40$$
$$C_D = 0.5, \qquad C_m = 0.5 \tag{27}$$

where the units are the same as those used in the Nomenclature. The material of the balloon film is chosen to be polyethylene, which has the following properties:

$$c_f = 2302.7, \qquad r_w = 0.127, \qquad r_{\text{wsol}} = 0.114, \qquad \alpha_w = 0.001$$
$$\epsilon_w = 0.031, \qquad \tau_w = 0.842, \qquad \tau_{\text{wsol}} = 0.885 \tag{28}$$

In conformity with Eq. (9), the linear wind field is assumed to be

$$\mathcal{U}_0 = 1.5, \qquad k_{11} = -0.001, \qquad k_{12} = 0.0, \qquad k_{13} = 0.005$$
$$\mathcal{V}_0 = 0.2, \qquad k_{21} = 0.004, \qquad k_{22} = -0.001, \qquad k_{23} = 0.003 \tag{29}$$

The velocity of the balloon in the x and y directions is approximated using Eq. (8) with $\gamma = 0.8$. The drag term in Eq. (13) is approximated using $k = 3$. This value of k conforms well with our simulation results where the vertical speed of the balloon satisfies $|\dot{z}| \leq \dot{z}_{\max} = 4$.

The rate of heat input to the balloon gas is chosen to be $\eta = 110,000$, assuming a fuel mass flow rate of 1 gm/s and a calorific value of 110 kJ/gm for the fuel. The initial states and the desired Cartesian coordinates of the balloon are assumed to be

$$\bar{x} = -2000, \quad \bar{y} = -3000, \quad \bar{z} = 0, \quad \dot{\bar{z}} = 0, \quad T_f = 250.0$$
$$T_g = 300.0, \quad x_d = 0, \quad y_d = 0, \quad z_d = 13{,}000 \tag{30}$$

As the first step of the algorithm discussed in Sec. IV.B, we perform a hover maneuver of the balloon in the neighborhood of its initial altitude to obtain a good first guess of the parameters in Eq. (18). From this maneuver, shown in Fig. 4, the following heat-flux parameters are obtained:

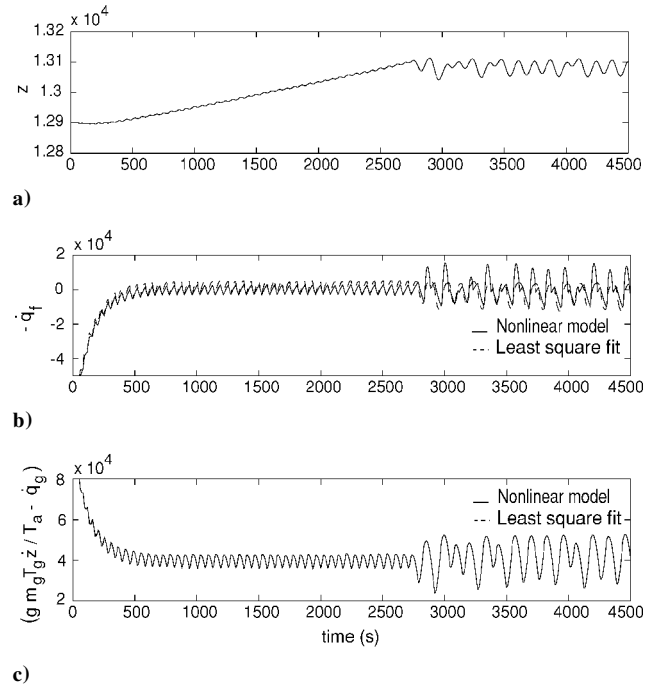

Fig. 4 Hover maneuver simulation for a good first estimate of the heat-flux parameters.

$$\bar{a}_1 = 0.013469, \qquad \bar{b}_1 = 0.006851, \qquad \bar{c}_1 = -0.000599$$
$$\bar{a}_2 = 0.139032, \qquad \bar{b}_2 = -0.042376 \qquad \bar{c}_2 = 0.003931 \tag{31}$$

As the second step of our algorithm, we solve the two-point boundary-value problem using the parameters in Eq. (31). The total time for simulation is $t_f = 1000$ s. The time step or mesh size is chosen as $h = 1$ s, which results in 1000 mesh points. Because the nonzero entries of the $\boldsymbol{F}$ matrix were chosen as unity, β is a measure of the fuel cost relative to the cost of terminal error. The value of β was selected to be 10^{-7}, which implies that the cost for continuous fuel consumption for the entire duration of flight is considered to be equivalent to a terminal error of $\phi = 10^6$, that is, an error of 1000 m in one of the Cartesian coordinates of the balloon. The results of simulation are shown in Fig. 5. The switching condition in Eq. (23) is satisfied for $\lambda_6 = -318.385$. It can be seen from Fig. 5a that switching occurs twice, at $t_1 = 97$ and at $t_2 = 498$. The input profile, which can be computed from Eq. (22), is shown in Fig. 5b.

We undertake the third step of our algorithm by simulating the motion of the balloon based on its nonlinear model and the input profile in Fig. 5b. The z trajectory of the balloon obtained from the nonlinear model is compared with the z trajectory obtained in step 2 of our algorithm. These trajectories, shown in Fig. 6, indicate the need for refinement of our linear dynamic model. To refine the linear dynamic model, we improve our estimates of the heat-flux parameters by using the z trajectory of the balloon obtained from the nonlinear model, shown in Fig. 6. This is based on step 4 of our algorithm, discussed in Sec. IV.B. The new parameter values are given here:

$$\bar{a}_1 = 0.025350, \qquad \bar{b}_1 = 0.009433, \qquad \bar{c}_1 = -0.000803$$
$$\bar{a}_2 = 0.146690, \qquad \bar{b}_2 = -0.040604, \qquad \bar{c}_2 = 0.003785 \tag{32}$$

Clearly, these values are not significantly different from the values in Eq. (31), which were used as the first estimates. It is also obvious from Fig. 7 that the new values provide a good linear approximation of the heat-flux expressions. In continuation of step 4 of our

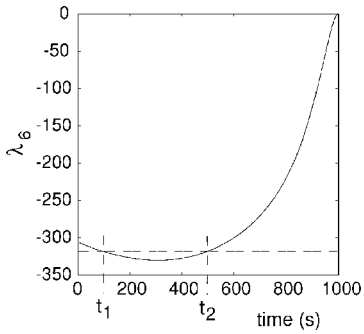

a)

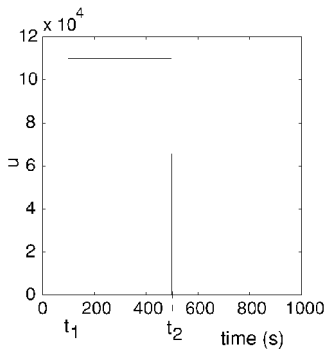

b)

Fig. 5 Switching condition and heat input profile obtained from the first run of the relaxation method.

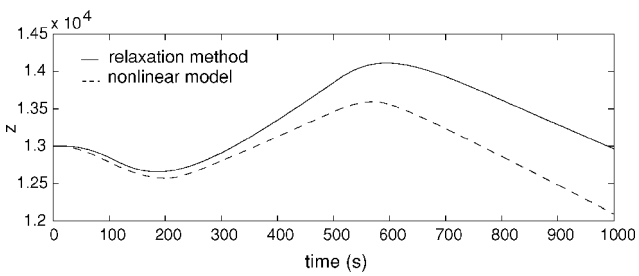

Fig. 6 Comparison of balloon z trajectories after the first run of the relaxation method.

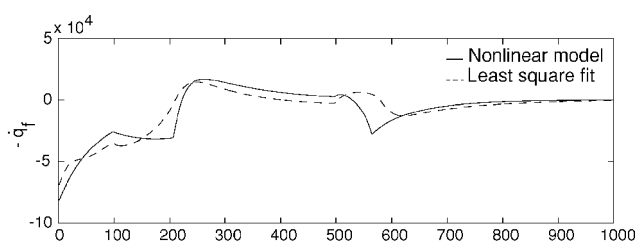

a)

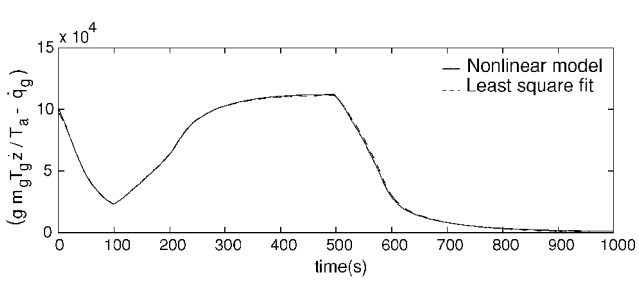

b)

Fig. 7 Least-squares fit for heat-flux terms after the first run of the relaxation method.

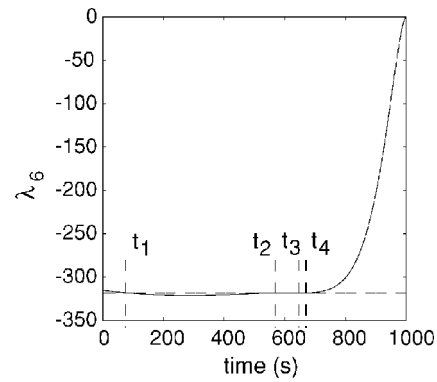

a)

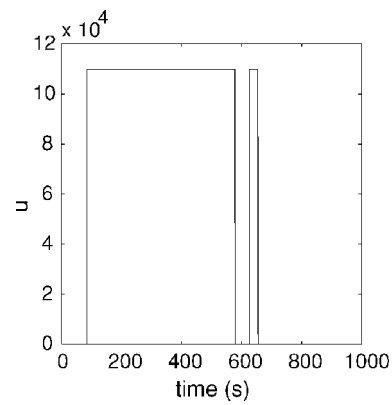

b)

Fig. 8 Switching condition and heat input profile obtained from the second run of the relaxation method.

algorithm, we run the relaxation algorithm with the new parameter values in Eq. (32). This results in the new input profile for the balloon, which is shown in Fig. 8b. The input profile is obtained from the trajectory of λ_6, shown in Fig. 8a. It is clear from Fig. 8 that the number of switchings have increased from two to four, and the new switching times are $t_1 = 85$, $t_2 = 579$, $t_3 = 626$, and $t_4 = 656$. To study the effect of model refinement, we simulate the nonlinear model of the balloon using the input profile in Fig. 8b. The results are shown in Fig. 9 in dotted lines. These results match very well with the results obtained from the second run of the relaxation method, shown in solid lines in Fig. 9. Because there is a good match between the trajectories, the input profile in Fig. 8b is considered to be optimal. The x, y, and z trajectories in Fig. 9 are therefore optimal with final coordinates

$$x = -176.43, \qquad y = -357.43, \qquad z = 12977.46 \tag{33}$$

The relaxation algorithm required 23 iterations and approximately 38 s to converge on a 1996 Sun Ultra-1 machine. Subsequently, refinement of the balloon dynamic model based on a single iteration of the heat-flux parameters yielded matching trajectories from the linear and nonlinear models. We have performed many such simulations and have consistently found that few iterations are required for convergence: most examples require one iteration, some require two, and we seldom require three or more iterations. In some cases our algorithm fails to provide convergence, but this occurs only for specific wind profiles. Except for these wind profiles, our algorithm provides a systematic framework for solving the intractable optimal control problem.

We conclude this section with a discussion on the wind profiles that render our algorithm inapplicable. Because the balloon is uncontrollable in x and y directions, our algorithm attempts to find a good match between the z trajectories of the balloon obtained from the linear and nonlinear models. It is implicitly assumed that a good match in the z trajectories will result in a good match in the x trajectories and the y trajectories. However, in some cases this

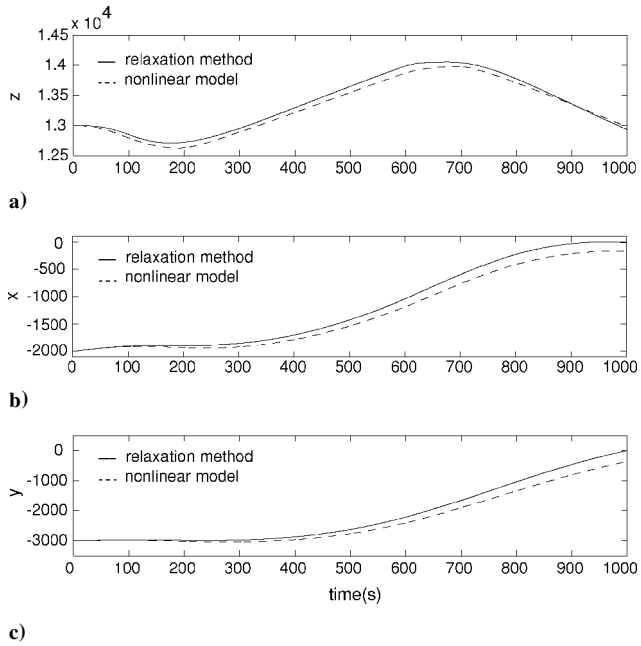

Fig. 9 Comparison of x, y, and z trajectories of the balloon after second run of the relaxation method.

assumption is not valid, and small errors between the z trajectories result in large differences between the x and y trajectories obtained from the linear and nonlinear models. To explain further, we use Eqs. (8) and (9) to express the motion of the balloon in x and y directions as follows:

$$\dot{x} = \gamma[\mathcal{U}_0 + k_{11}(x - x_0) + k_{12}(y - y_0) + k_{13}(z - z_0)] \quad (34a)$$

$$\dot{y} = \gamma[\mathcal{V}_0 + k_{21}(x - x_0) + k_{22}(y - y_0) + k_{23}(z - z_0)] \quad (34b)$$

If we now denote the x, y, z trajectories of the balloon obtained from the nonlinear model as reference trajectories x_r, y_r, z_r, we can rewrite Eq. (34) with x, y, z replaced by x_r, y_r, z_r. By subtracting this equation from Eq. (34), we get

$$\begin{bmatrix} \dot{\hat{x}} \\ \dot{\hat{y}} \end{bmatrix} = \gamma \begin{bmatrix} k_{11} & k_{12} \\ k_{21} & k_{22} \end{bmatrix} \begin{bmatrix} \hat{x} \\ \hat{y} \end{bmatrix} + \gamma \begin{bmatrix} k_{13} \\ k_{23} \end{bmatrix} \hat{z} \quad (35)$$

where $\hat{x} \triangleq (x - x_r)$, $\hat{y} \triangleq (y - y_r)$, and $\hat{z} \triangleq (z - z_r)$ are x, y, and z trajectories of the balloon obtained from the linear model expressed relative to the reference trajectories. It now becomes obvious that the x and y trajectories obtained from the linear model can diverge from those obtained from the nonlinear model when eigenvalues of the 2×2 matrix in Eq. (35) have positive real parts. On the contrary, when the matrix is Hurwitz, bounds on $\hat{x}$ and $\hat{y}$ will be proportional to the bound on $\hat{z}$. This essentially implies that a good match between the z trajectories obtained from the linear and nonlinear models will ensure a good match in the x trajectories and y trajectories.

VI. Conclusion

A hot-air balloon is a complex dynamical system with unidirectional control of its altitude. It does not have direct control of its motion in the horizontal plane and has to ride the wind field judiciously to move toward a target location. In this paper we address the optimal control problem with the objective of designing trajectories of the balloon that minimize a weighted sum of its terminal error and fuel consumption. The problem is intractable because of the nonlinear thermodynamic model of the balloon and switching nature of the heat input. An analytical solution to the problem does not exist, and a numerical solution is elusive. Using a nontraditional approach for linearization, we simplify the balloon dynamic model and numerically solve the ensuing two-point boundary-value problem. We refine the simplified model and using an iterative approach, which requires very few iterations, obtain accurate optimal trajectories. Unfortunately, our algorithm fails to converge when eigenvalues of the wind field have positive real parts. This somewhat limits the usefulness of our approach, but considering the intractable and elusive nature of the problem it achieves a modest level of success in our first attempt at problem resolution. A complete resolution of the problem will require additional work that allows us to plan trajectories with arbitrary wind fields as well as wind fields described by statistical data. The long-term goal of our research is to study the optimal control problem in other balloon systems, such as balloons using phase change fluids, that will find applications in planetary exploration.

Appendix: Balloon Heat Transfer

The convective heat-transfer coefficients CH_{fa} and CH_{gf} in Eqs. (5) and (6) can be expressed as follows:

$$CH_{\text{fa}} = Nu_a K_a / 2\bar{R}, \qquad CH_{\text{gf}} = Nu_g K_g / 2\bar{R} \quad (A1)$$

where the thermal conductivities K_a and K_g are given by the relations

$$K_a = 1.99 \times 10^{-3} \left(\frac{T_a^{1.5}}{T_a + 112.0} \right)$$

$$K_g = 1.99 \times 10^{-3} \left(\frac{T_g^{1.5}}{T_g + 112.0} \right) \quad (A2)$$

In Eq. (A1) Nu_a and Nu_g are computed from the values of Gr_a, Gr_g, Re, and Pr. Whereas Pr has a constant value of 0.72, Gr_a, Gr_g, and Re vary according to the following relations:

$$Gr_a = g\rho_a^2 \frac{(T_f - T_a)\bar{R}^3}{T_a \mu_a^2}, \qquad Gr_g = g\rho_g^2 \frac{(T_g - T_f)\bar{R}^3}{T_g \mu_g^2}$$

$$Re = 2\dot{z} \frac{\bar{R}\rho_a}{\mu_a} \quad (A3)$$

where

$$\rho_a = \frac{p_a M_a}{R T_a}, \qquad \rho_g = \frac{p_a M_a}{R T_g}$$

$$\mu_a = 1.49 \times 10^{-6} \left(\frac{T_a^{1.5}}{T_a + 112.0} \right)$$

$$\mu_g = 1.49 \times 10^{-6} \left(\frac{T_g^{1.5}}{T_g + 112.0} \right) \quad (A4)$$

and

$$T_a = \begin{cases} T_{\text{inv}} & \text{if} \quad z < z_{\text{inv}} \\ T_{\text{sea}} - 0.00651 z & \text{if} \quad z_{\text{inv}} \le z < z_{\text{trop}} \\ T_{\text{strat}} & \text{if} \quad z \ge z_{\text{trop}} \end{cases}$$

$$p_a = \begin{cases} (8.966 - 0.0002025 z)^{5.256} & \text{if} \quad z < z_{\text{trop}} \\ p_{\text{trop}} e^{(1.69 - 0.000157\, z)} & \text{if} \quad z \ge z_{\text{trop}} \end{cases} \quad (A5)$$

where standard values of T_{inv}, T_{sea}, T_{strat}, z_{inv}, z_{trop}, and p_{trop} are as follows:

$$T_{\text{inv}} = 282.0, \qquad T_{\text{sea}} = 288.15, \qquad T_{\text{strat}} = 214.4$$

$$z_{\text{inv}} = 944.7, \qquad z_{\text{trop}} = 10769.0, \qquad p_{\text{trop}} = 23502.0$$

Using Eqs. (A3) and (A4), Nu_a and Nu_g can now be computed as follows:

$$Nu_a = \max[(Nu_a)_1, (Nu_a)_2]$$

$$Nu_g = \begin{cases} 0.325(Gr_g Pr)^{\frac{1}{3}} & \text{if} \quad (Gr_g Pr) > 1.34681 \times 10^{-8} \\ 2.5\left[2.0 + 0.6(Gr_g Pr)^{\frac{1}{4}}\right] & \text{if} \quad (Gr_g Pr) \le 1.34681 \times 10^{-8} \end{cases} \tag{A6}$$

where $(Nu_a)_1$ and $(Nu_a)_2$ are defined as

$$(Nu_a)_1 = \begin{cases} 0.37Re^{0.6} & \text{if} \quad V < V_{\text{cr}} \\ 0.74Re^{0.6} & \text{if} \quad V \ge V_{\text{cr}} \end{cases}, \qquad \begin{aligned} V_{\text{cr}} &= 538000.0 \\ (Nu_a)_2 &= 2.0 + 0.6(Gr_g Pr)^{\frac{1}{4}} \end{aligned} \tag{A7}$$

The emmissivity of the balloon gas in the infrared spectrum ϵ_g, appearing in Eq. (7), is given by the relation

$$\epsilon_g = 0.169\left(1.746 \times 10^{-6} T_g\right)^{0.8152} \tag{A8}$$

Equations (A1–A8), together with Eqs. (1–9) in the main body of the paper, are representative of the nonlinear model of the balloon.

Acknowledgment

The first two authors gratefully acknowledge the support provided by NASA Jet Propulsion Laboratory, JPL Contract 1216050, in conducting this research.

References

[1]Kreider, J. F., "Mathematical Modeling of High Altitude Balloon Performance," AIAA Paper 75-1385, 1975.

[2]Kreith, F., and Kreider, J. F., "Numerical Prediction of the Performance of High Altitude Balloons," National Center for Atmospheric Research, NCAR Technical Note, NCAR-IN/STR-65, Boulder, CO, 1971.

[3]Carlson, L. A., and Horn, W. J., "New Thermal and Trajectory Model for High-Altitude Balloons," *Journal of Aircraft*, Vol. 20, No. 6, 1983, pp. 500–507.

[4]Wu, J. J., and Jones, J. A., "Performance Models for Reversible Fluid Balloons," AIAA Paper 95-1623, May 1995.

[5]Scheid, R. E., Heun, M. K., Cameron, J. M., and Jones, J. A., "Thermodynamics, Phase Change, and Mass Transfer in Oscillatory Balloon Systems (Aerobots)," AIAA Paper 96-1870, June 1996.

[6]Aaron, K. M., Heun, M. K., and Nock, K. T., "Balloon Trajectory Control," AIAA Paper 99-3865, Aug. 1999.

[7]Folta, D., Newman, L., and Gardner, T., "Foundations of Formation Flying for Mission to Planet Earth and the New Millennium," AIAA Paper 96-3645, July 1996.

[8]Press, W. H., Teukolsky, S. A., Vetterling, W. T., and Flannery, B. P., *Numerical Recipes in C*, Cambridge Univ. Press, New York, 1992, p. 762.

[9]Lewis, F. L., and Syrmos, V. L., *Optimal Control*, Wiley, New York, 1995, p. 153.

[10]Kreyzig, E., *Advanced Engineering Mathematics*, Wiley, New York, 1993, p. 1001.

[11]Leitmann, G., *An Introduction to Optimal Control*, McGraw–Hill, New York, 1966, pp. 46, 47.

[12]Lu, P., Sun, H., and Tsai, B., "Closed-Loop Endo-Atmospheric Ascent Guidance," AIAA Paper 2002-4558, Aug. 2002.